Fabrication of thin-film thermoelectric generators with ball lenses for conversion of near-infrared solar light

Yoshitaka Ito[1], Mizue Mizoshiri[1]*, Masashi Mikami[2], Tasuku Kondo[1], Junpei Sakurai[1], and Seiichi Hata[1]

[1]*Department of Micro-Nano Systems Engineering, Graduate School of Engineering, Nagoya University, Nagoya 464-8603, Japan*

[2]*National Institute of Advanced Industrial Science and Technology, Nagoya 463-8560, Japan*

E-mail: mizoshiri@mech.nagoya-u.ac.jp

We designed and fabricated thin-film thermoelectric generators (TEGs) with ball lenses which separated the visible and the near-infrared (NIR) solar light using a chromatic aberration. The transmitted visible light was used as daylight and the NIR light was used for thermoelectric generation. Solar light was estimated to be separated visible and NIR light by a ray tracing method. 92.7% of the visible light was used for daylight and 9.9% of the NIR light was used for generation. Then, the temperature difference of the pn junctions of the TEGs surface was 0.71K by the heat conduction analysis using a finite element method. The thin-film TEGs were fabricated by using lithography and deposition process. When the solar light (A.M. 1.5) was irradiated to the TEGs, the open-circuit voltage and maximum power were 4.5 V/m^2 and 51 μW/m^2, respectively. This TEGs is expected to be used as energy supply for IoT sensors.

1. Introduction

Recently, energy harvesting devices have attracted attention in Internet of Things (IoT) and Trillion Sensors Universe to supply electric power to the IoT sensors.[1, 2] These devices, which generate several hundreds of microwatts used with storage systems, convert waste energy in environment into electric energy. Ambient energy sources such as vibration, light, and heat are used for energy harvesting. For example, vibration energy is converted to electric energy by piezoelastic devices.[3-7] Light energy such as solar and artificial light is converted to electric energy using photovoltaic cells.[8-12] Thermal energy creates temperature gradient which is converted to electric energy using thermoelectric generators (TEGs).[13-23]

Solar light is a promising renewable energy which has a wide spectrum from the ultraviolet to the near-infrared (NIR) light. The visible light which is approximately 53% of solar light is used as daylight in our lives and is converted to electric energy using photovoltaic generation systems. However, the NIR light which is approximately 42% of solar light cannot be efficiently converted into electric energy using photovoltaic effect. Moreover, the conversion efficiency of c-Si photovoltaic cells is decreased with increasing the cells' temperature by the irradiation of the NIR light.[24, 25]

To use the NIR solar light effectively, thermal-photovoltaic hybrid generators have been reported. The hybrid generators, which compose of photovoltaic cells and TEGs, converted the visible light and the NIR light into electric energy using photovoltaic effect and thermoelectric (TE) effect, respectively.[26-30] It is important for TEGs to create a large temperature gradient between hot sides and cold sides of pn junctions because the generation voltage is linearly increased with temperature gradient and the generation power is increased with the square of the temperature gradient.

Thin-film TEGs can be classified into two types: a vertical type and a planar type. In the vertical type, the temperature gradient is created in the thickness direction of the thin-film TE elements. On the other hand, the planar type TEGs convert the temperature gradient into the thin-film TE elements to electric energy. In thin-film TEGs, it is difficult to improve the generation performance of the vertical type because a large temperature gradient cannot be generated into the thin films in the thickness.[13-17] In the planar type, the temperature gradient enables to be controlled by changing the length of the TE elements.[18-23] To date, we have also fabricated thermal-photovoltaic hybrid generators which composed of thin-

film TEGs and commercially-available photovoltaic cells, hot mirrors, and focal lenses. The thin-film TEGs converted the NIR solar light which was separated from full solar light. The NIR light was focused onto the hot sides of thin-film TEGs using the focal lens. However, the hybrid generators are relatively large volume to set on the IoT sensors and ambient goods such as windows because they composed the bulk mirrors and lenses. If small and visibly transparent TEGs are developed, the NIR light enables to be used as an energy source effectively and the visible light enables to be used as daylight when the TEGs are set on the transparent materials.

In this study, we proposed visibly transparent thin-film TEGs with small ball lenses that enabled to be used by setting on glass windows. The thin-film TEGs with ball lenses were designed to transmit the visible light and convert the NIR light to electric energy using a chromatic aberration induced by the small ball lens. In the calculation using a ray tracing method and a finite element method (FEM), the TEGs with pinholes and the ball lenses which separated the visible light and the NIR light using the chromatic aberration were designed. The ball lenses focused the NIR light onto the hot sides of the TEGs and transmitted the visible light to the glass substrate. Then, we demonstrated the fabrication of the TEGs with ball lenses and evaluated the generation properties.

2. Design of thermoelectric generator

2.1 Design concept

Figure 1 shows a schematic illustration of the thin-film TEGs with small ball lenses. The TEGs were serially-connected as shown in Fig.1(a) to generate large voltage. The number of the TEGs were 111. The small ball lenses were set on a center of a pinhole. When the ball lenses were focused full solar light, it light was separated into the visible light and the NIR light by using chromatic aberration of the wavelength dependence. The visible light was focused onto the center of the pair of pn junction which passed through the transparent glass substrate. The visible light was used for daylight. In contrast, the NIR light was defocused and irradiated onto the hot side of the TE elements as shown in Fig. 1(b). The temperature gradient between the hot side of center of the TE elements and the cold side of the circumference of the TE elements was generated TE voltage.

2.2 Simulation method

Theoretical analysis of focusing properties of solar light using the small ball lenses was performed using a ray tracing method (OSLO EDU) which geometrically calculated the path of the light propagation depended on wavelength. The simulation models and parameters were shown in Fig. 2 (a) and Table I, respectively. The radius of a pinhole was determined as $1/e^2$ radius of the focal spot at the maximum visible wavelength (assumed as 800 nm) because the focal spot was increased with increasing wavelength. The pinhole radius was 26 μm by taking account of the calculation result.

An energy which passed though the pinhole at a wavelength in the solar light λ was defined as $E_t(\lambda)$ and the solar energy at the wavelength λ was defined as $E(\lambda)$. Then, the transmittance $t(\lambda)$ though the pinhole at the wavelength λ was described using the following equation (1):

$$t(\lambda) = \frac{E_t(\lambda)}{E(\lambda)}. \qquad (1)$$

The transmittance of the visible solar light at wavelength from 280 to 800 nm, T_{vis}, as follows:

$$T_{vis} = \int_{\lambda=280nm}^{\lambda=800nm} t(\lambda) = \int_{\lambda=280nm}^{\lambda=800nm} \frac{E_t(\lambda)}{E(\lambda)}. \qquad (2)$$

If the all visible solar light at wavelength from 280 to 800 nm was transmitted inside the pinhole, T_{vis}, was 100%.

The irradiated rate of NIR solar light at wavelength from 800 to 4000 nm, U_{NIR}, was described as follows:

$$U_{NIR} = \int_{\lambda=800nm}^{\lambda=4000nm} 1-t(\lambda) = \int_{\lambda=800nm}^{\lambda=4000nm} \frac{E(\lambda)-E_t(\lambda)}{E(\lambda)}. \qquad (3)$$

Temperature gradient of the thin-film TEGs was calculated using a FEM heat conduction analysis (COMSOL Multiphysics). The heat flux by the NIR solar light which exhibited different focal spot radius depended on the wavelength was assumed by considering each focal spot diameter and solar light energy at the wavelength. The focal spot radius was determined as $1/e^2$ radius of the focal spot at each wavelength. The both visible light (280–800 nm) and NIR light (800–4000 nm) which were irradiated to inside the pinhole were transmitted through the glass substrate. The transparency of the both light was decided

to be 90%, which was experimentally obtained. Therefore, 10% of the irradiated energy to inside the pinhole was assumed to be absorbed by the glass substrate. In contrast, 100% of the visible and the NIR light which were irradiated to outside the pinhole were assumed to be absorbed by the electrode and TE elements, and be converted into thermal energy without energy loss. The temperature distribution at steady state was calculated. The commercially-available small ball lenses (sapphire, Edmund Optics) were used in the TEGs. Materials of the TEGs were as follows. $Bi_{0.5}Sb_{1.5}Te_3$ and $Bi_2Te_{2.7}Se_{0.3}$ were used as p-type and n-type thin-film TE elements. Cu thin films was used as the electrodes. It is expected that the temperature difference underlying Cu electrodes cannot contribute to the thermoelectric generation because the TE elements form a closed circuit with Cu electrodes. Therefore, the width of Cu electrodes was decided to be 50 μm, which was fine and exhibited small resistance. SiO_2 thin films were overcoated on the TE elements and the electrodes to prevent oxidization. Table II shows the material properties. Figure 2(b) exhibited the two-dimensional model of the cross-sectional of the TEGs for the heat conduction analysis. The boundary conditions on center and circumference lines were determined as heat insurance because the TEGs were periodically formed as shown in Fig. 1(a). The other boundaries were defined as natural conversion. The heat transfer coefficient was decided as 5 W/m^2K. The minimum and maximum mesh sizes in FEM were 20 nm and 10 μm, respectively.

2.3 Simulation result of TEGs

Figure 3 (a) shows two of the all calculated intensity distributions of focused solar light at 800 nm wavelength and 2703 nm wavelength. The visible (800 nm) and NIR (2703 nm) solar light enabled to be separated using a chromatic aberration induced by the ball lens when the pinhole radius was 26 μm. 92.9% of the energy at 800 nm wavelength (the intensity distribution hatched with the thin blue line) was used for daylight and 20.5% of the energy at 2703 nm wavelength (the intensity distribution hatched with the bold red line) was used for generation. As the results of the all calculations at visible to NIR solar light wavelength by the ray tracing method, it was found that the transparency of the visible light of 280−800 nm to the pair of pn junctions was 92.7%. 9.9% of the NIR light was estimated to be irradiated to generate electric power. Figure 3(b) shows the temperature distribution of the device surface. When the length of the TE elements was 374 μm from the radial position at

76 μm to 450 μm, the maximum temperature difference was estimated as 0.71K.

3. Fabrication methods

Thin-film TEGs were fabricated using lithography and deposition process. The schematic illustration of the fabrication process was shown in Fig. 4. A chemically-amplified positive-tone photoresist (PMER P-CA1000PM, Tokyo Ohka Kogyo) was spin-coated on the glass substrate. The thickness of the substrate was 200 μm. P-type TE thin-film of $Bi_2Te_{2.7}Se_{0.3}$ with 1 μm thickness was deposited on the substrate by radio-frequency (RF) magnetron sputtering method. After that, the resist patterns were removed using acetone. N-type thin-film TE elements of $Bi_2Te_{2.7}Se_{0.3}$ with 1 μm thickness was also formed using the same process as the n-type thin-film TE elements. Then, thermal treatment was conducted at 623K for 3 hours in vacuum atmosphere to improve the crystallinity. To connect the thin-film TE elements, the resist patterns were formed and Cu thin films with 500 nm thickness were deposited by the sputtering method. Buffer layer of Cr with 2 nm thickness was used underlying $Bi_2Te_{2.7}Se_{0.3}$, $Bi_2Te_{2.7}Se_{0.3}$ and Cu patterns. After the resist removal, SiO_2 thin-film with 200 nm was coated onto the TE films and the Cu films. Finally, the resist patterns were formed to align the ball lenses, following that the ball lenses were put on the center of the TEGs with tweezers. Generation voltage of a pair of the pn junction was 216 μV/K, which was the average value at 303–323K. The electrical conductivity of the TE films (10mm × 0.5 mm) were 1250 S/cm (p-type) and 509 S/cm (n-type), respectively.

4. Results and discussion

4.1 Fabrication of thermoelectric generators

Figures 5(a) and 5(b) show an optical microscope image and a photograph of the TEGs with the small ball lenses, respectively. The thin-film TE elements was electrically-connected. The total electrical resistance (111 pairs of the pn junctions) was 2.50 kΩ. The theoretical resistance calculated without the resistance of the contact and Cu electrodes was 1.84 kΩ using the resistivity of TE and Cu thin films. It indicates that the contact and Cu electrodes' resistance estimated to be 0.66 kΩ. Here, the lenses were not fixed on the TEGs to evaluate the generation properties simply. However, it is also possible to fix the lenses by reflowing the resist for the alignment.

4.2 Evaluation of thermoelectric generators

The generation properties of the TEGs with ball lenses were evaluated. The electrical resistance of serially-connected one line (7 TEGs) was 158 Ω. Figure 6(a) and 6(b) show the generation properties when a solar light (A.M.1.5) was irradiated at 298K. The open-circuit voltage and maximum power were 0.88 mV and 1.0 nW, respectively. The temperature difference between the hot side and the cold side (distance: 374 μm) was estimated as 0.58K using Seebeck coefficient of the thin-films TE elements. The open-circuit voltage and maximum power per unit area were 4.5 V/m^2 and 51 μW/m^2, respectively. The designed maximum power was 126 μW/m^2 which was calculated using the values the electrical resistivity and Seebeck coefficients of the p- and n-type TE films, and the temperature difference between the hot sides and cold sides. The internal resistance of the fabricated TEG was 22.5 Ω which was approximately 1.4 times larger than that of the designed one of 16.6 Ω. Furthermore, the generation voltage of the fabricated TEG was 0.82 times of the estimated one using Seebeck coefficient of the TE films and the temperature difference. These results agreed with the reduction of the generated power. Although the generation power was smaller than the designed one, the order of this generation power per unit area is enough to use on the glass windows with the size of sub square meter because millivolt-ordered voltage can be charged to the battery.

4. Conclusion

Thin-film TEGs with small ball lenses were fabricated and evaluated. The design of the TEGs were conducted using ray tracing method to calculate solar light propagation and using FEM for heat conduction analysis. When the pinhole radius was 26 μm, the visible light transparency was estimated as 92.7% for daylight and the 9.9% of the NIR light was estimated to generate the temperature difference of 0.71K between hot side and cold side. The electrical internal resistance of the fabricated TEGs was 2.50 kΩ. The open-circuit voltage and the maximum generation power were 4.5 V/m^2 and 51 μW/m^2, respectively.

Acknowledgments

This study was partially supported by the Nanotechnology Platform Program (Micro-Nano

Fabrication) of the Ministry of Education, Culture, Sports, Science and Technology, Japan, JSPS KAKENHI Grant Number 15K13845, and the Asahi Glass Foundation.

References

1) J. Gubbi, R. Buyya, S. Marusic and M. Palaniswami, Fut. Gen. Comput. Sys. **29** 1645 (2013)
2) A. Zanella, N. Bui, A. Castellani, L. Vangelista, M. Zorzi, IEEE Internet Things J. **1** 22 (2014)
3) S. P. Beeby, R. N. Torah, M. J. Tudor, P. Glynne-jones, T. O'Donnell, C. R. Saha and S. Roy, J. Micromech. Microeng. **17** 1257 (2007)
4) V. R. Challa, M. G. Prasad, Y. Shi and F. T. Fisher, Smart Mater. Struct. **17** 015035 (2008)
5) H. B. Fang, J. Q. Liu, Z. Y. Xu, L. Dong, L. Wang, D. Chen, B. C. Cai and Y. Liu, Microelectronics J. **37** 1280 (2006)
6) E. S. Leland and P. K. Wright, Smart Mater. Struct. **15** 1413 (2006)
7) H. W. Kim, A. Batra, S. Priya, K. Uchino, D. Markley, R. E. Newnham and H. F. Hofmann, Jpn. J. Appl. Phys. 43 6178 (2004)
8) M. Gra1tzel, Inorg. Chem. **44** 6841 (2005)
9) P. V. Kamat, J. Phys. Chem. C **112** 18737 (2008)
10) X. Gu, X. Yu, K. Guo, L. Chen, D. Wang and D. Yang, Sol. Energy Mater. Sol. Cells **101** 95 (2012)
11) T. Stelzner, M. Pietsch, G. Andra, F. Falk, E. Ose and S. Christiansen, Nanotechnology **19** 295203 (2008)
12) H. Jabbar, Y. S. Song and T. T. Jeong, IEEE Trans. Cons. Electron. **56** 247 (2010)
13) K. H. Lee and O. J. Kim, Int J. Heat Mass Transfer **50** 1982 (2007)
14) Z. Wang, V. Leonov, P. Fiorini and C. V. Hoof, Sens. Actuators A **156** 95 (2009)
15) R. Amatya and R. J. Ram, J. Electron. Mater. **39** 1735 (2010)
16) G. J. Snyder, J. R. Lin, C. Huang and J. P. Fleurial, Nat. Mater. **2** 528 (2003)
17) M. K. Kim, M. S. Kim, S. Lee, C. Kim and Y. J. Kim, Smart Mater. Struct. **23** 105002 (2014)
18) J. Su, V. Leonov, M. Goedbloed, Y. V. Andel, M. C. D. Nooijer, R. Elfrink, Z. Wang and R. J. M. Vullers, J. Micromech. Microeng. **20** 104005 (2010)

19) J. Weber, K. Potje-Kamloth, F. Hasse, P. Detemple, F. Volklein and T. Doll, Sens. Actuators A **132** 325 (2006)
20) S. M. Yang, T. Lee and M. Cong, Sens. Actuators A **157** 258 (2010)
21) P. Li, L. Cai, P. Zhai, X. Tang, Q. Zhang and M. Niino, J. Electron. Mater. **39** 1522 (2010)
22) M. Takashiri, T. Shirakawa, K. Miyazaki and H. Tsukamoto, Sens. Actuators A **138** 329 (2007)
23) D. Kraemer, B. Poudel, H. P. Feng, J. C. Caylor, B. Yu, X. Yan, Y. Ma, X. Wang, D. Wang, A. Muto, K. McEnaney, M. Chiesa, Z. Ren and G. Chen, Nat. Mater. **10** 532 (2011)
24) E. Skoplaki and J. A. Palyvos, Sol. Energy **83** 614 (2009)
25) B. Rech and H. Wagner, Appl. Phys. A **69** 155 (1999)
26) W. G. J. H. M. V. Sark, Appl. Energy **88** 2785 (2011)
27) N. Wang, L. Han, H. He, N. H. Park and K. Koumoto, Energy Environ. Sci. **4** 3676 (2011)
28) P. Li, L. Cai, P. Zhai, X. Tang, Q. Zhang and M.Niino, J. Electron. Mater. **39** 1522 (2010)
29) X. Ju, Z. Wang, G. Flamant, P. Li and W. Zhao, Sol. Energy **86** 1941 (2012)
30) M. Mizoshiri, M. Mikami and K. Ozaki, Jpn. J. Appl. Phys. **51** 06FL07 (2012)

Figure Captions

Fig. 1 Schematic illustrations of (a) thin-film TEGs and (b) one TEG with a ball lens.

Fig. 2 Schematic illustrations of (a) a thin-film TEG and solar light propagation. (b) The cross-sectional view of the TEGs and sizes.

Fig. 3 (Color online) (a) Intensity distributions on the surface of a pair of pn junctions at wavelength of 800 nm (a visible wavelength) and 2703 nm (a NIR wavelength). (b) The temperature distribution on the surface of a pair of pn junctions when full solar light irradiated using the ball lens.

Fig. 4 Schematic illustration of fabrication process for thin-film TEGs.

Fig. 5 (Color online) (a) Optical microscope image and (b) photograph of the TEGs with ball lenses.

Fig. 6 Generation properties of the serially-connected 7 TEGs: (a)voltage and current diagram, and (b)power and current diagram.

Table I. Ray tracing method condition.

Lens diameter (μm)	Lens refractive index	Wavelength (nm)	Device diameter (μm)
1000	1.77	280-4000	1000

Table II. Material property for heat conduction analysis.

	Thermal conductivity (W/m k)	Density (kg/m^3)	Specific heat capacity (J/ kg K)
TE element	1.0	7000	170
Cu	400	8700	385
SiO_2	1.38	2203	703

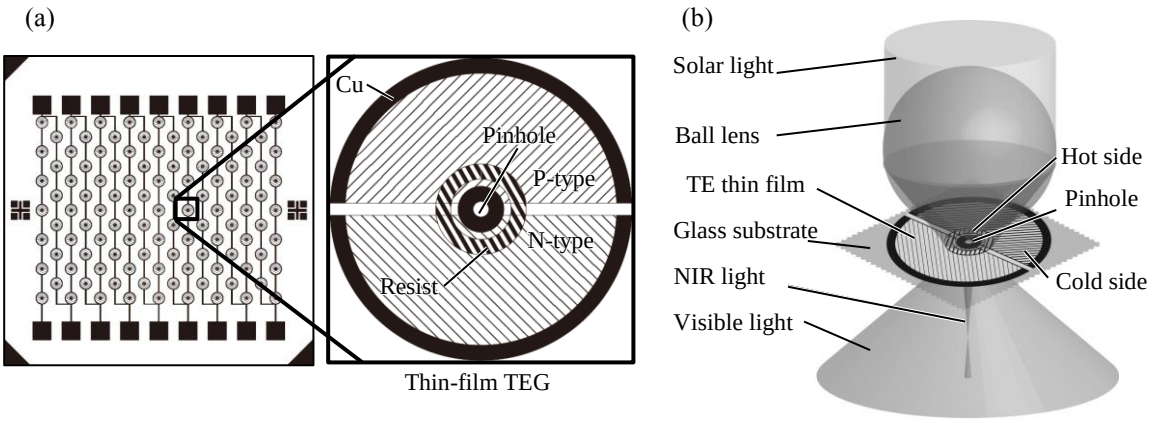

Fig. 1 Schematic illustrations of (a) thin-film TEGs and (b) one TEG with a ball lens.

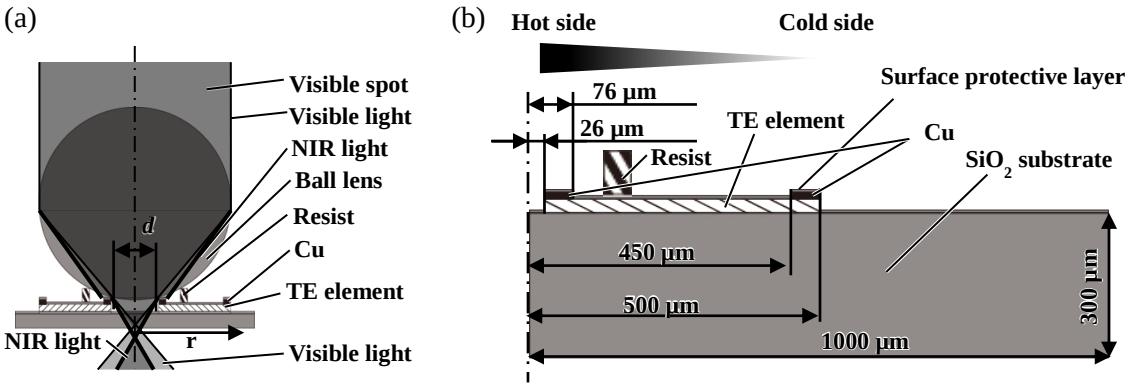

Fig. 2 Schematic illustrations of (a) a thin-film TEG and solar light propagation. (b) The cross-sectional view of the TEGs and sizes.

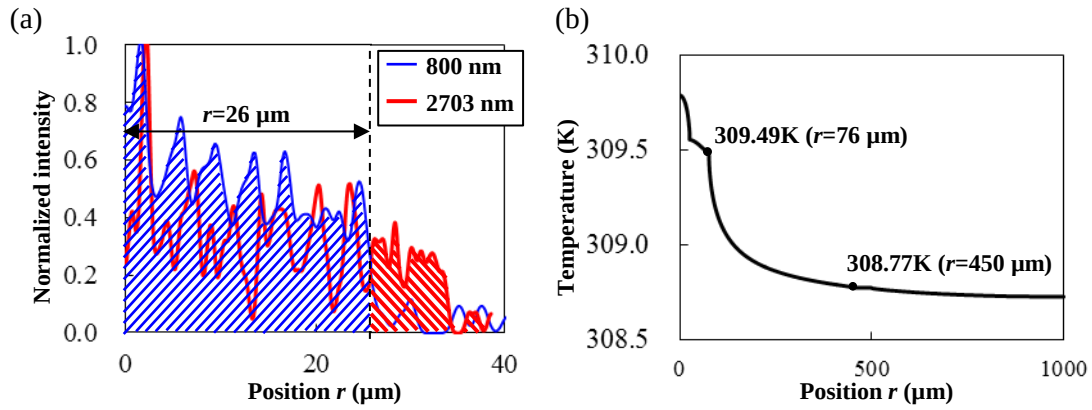

Fig. 3 (Color online) (a) Intensity distributions on the surface of a pair of pn junctions at wavelength of 800 nm (a visible wavelength) and 2703 nm (a NIR wavelength). (b) The temperature distribution on the surface of a pair of pn junctions when full solar light irradiated using the ball lens.

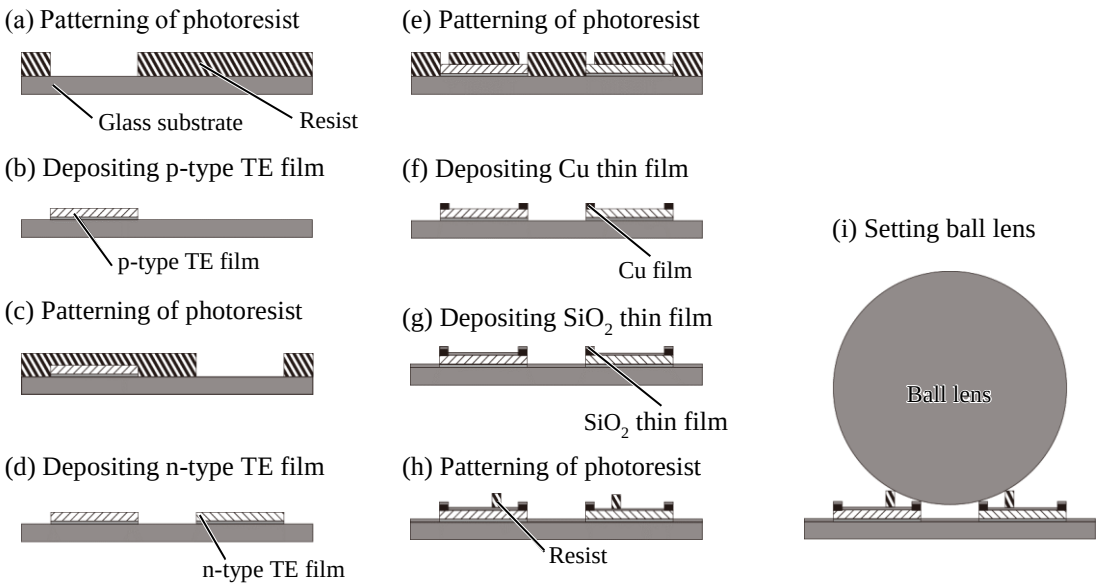

Fig. 4 Schematic illustration of fabrication process for thin-film TEGs.

(a) (b)

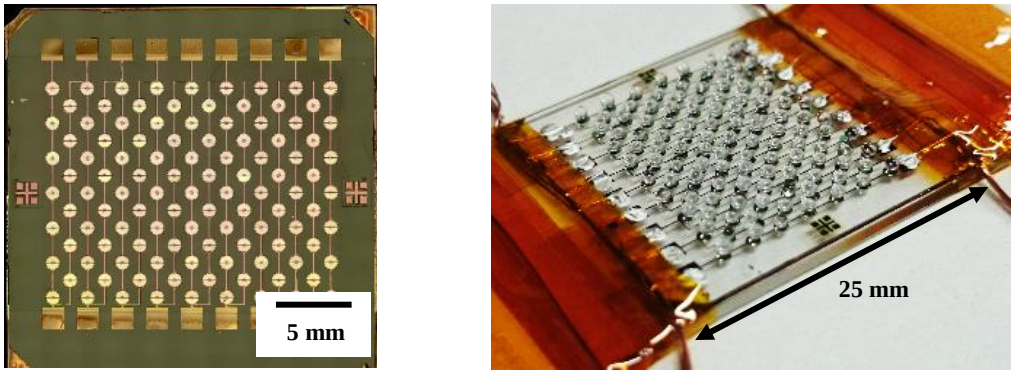

Fig. 5 (Color online) (a) Optical microscope image and (b) photograph of the TEGs with ball lenses.

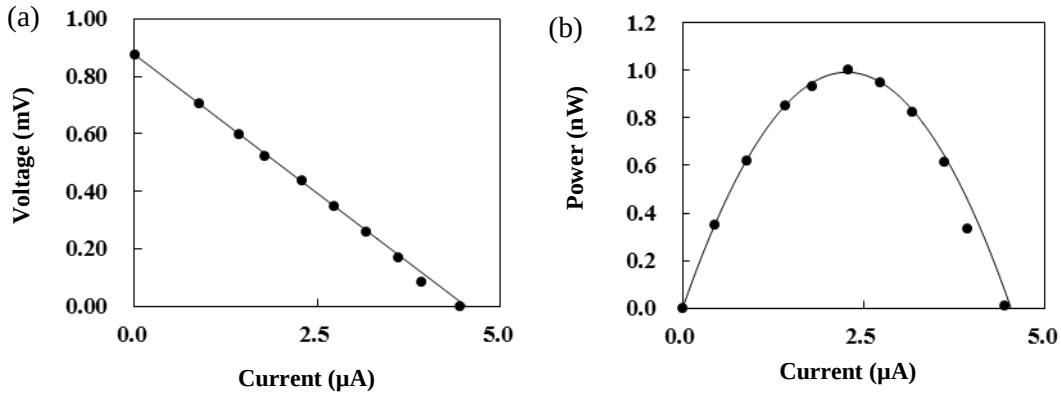

Fig. 6 Generation properties of the serially-connected 7 TEGs: (a)voltage and current diagram, and (b)power and current diagram.